Computational Study on the Stacking Interaction in Catechol Complexes

Laura Estévez, Nicolás Otero, and Ricardo A. Mosquera*

Departamento de Química Física, Facultade de Química, Universidade de Vigo, Lagoas-Marcosende s/n 36310-Vigo, Galicia, Spain

Received: June 28, 2009

The stability and electron density topology of catechol complexes (dimers and tetramer) were studied using the MPW1B95 functional. The QTAIM analysis shows that both dimers (face to face and C−H/π one) display a different electronic origin. The formation of the former is accompanied by a significant change in the values of atomic electron dipole and quadrupole components, flattening the most diffuse part of the electron density distribution toward the molecular plane. A small electron population transfer is observed between catechol monomers connected by C−H/π interactions, whose QTAIM characterization does not differ from that of a weak hydrogen bond. Cooperative effects in the tetramer on binding energies are small and negligible for bond properties and charge transfer. Nevertheless, they are significant on atomic electron populations.

Introduction

Molecules containing π-delocalized systems can participate in a wide series of noncovalent weak bonds comprising $\pi-\pi$, X−H/π, and cation−π interactions.[1] The term stacking interaction is sometimes used to include all of them, whereas it is also common to find it is restricted to designate $\pi-\pi$ interactions leading to the formation of a complex or adduct consisting of piled up monomers. It is considered that stacking interactions, both in wide or restricted sense, are key factors in determining the structure of biomacromolecules including DNA and supramolecular systems and play leading roles in molecular recognition processes.[2−5] Therefore, they have attracted considerable interest (for a recent revision see ref 4). Nevertheless, the computational treatment of these systems is not straightforward as their description requires an accurate description of dispersion forces, which are important or even dominant in many of these interactions. This problem has only recently become affordable at computational levels viable for medium/large size systems with the advent of new density functional theory (DFT) functionals,[6] like the kinetics-optimized ones developed by Zhao and Truhlar.[7,8] For this reason, the literature on electron density analysis of stacking interaction is still scarce,[9−12] and more studies are needed to get insight into the electronic origin of these interactions.

Furthermore, the weak attraction between C−H bonds and π systems was often described as the weakest class of conventional hydrogen bonds. Nevertheless, in a recent revision[13] where theoretical and spectroscopic studies are discussed in detail, the authors notice that, although the electrostatic interaction is mainly responsible for the attraction in the conventional hydrogen bonds,[14−17] dispersion can be recognized as the major source of attraction between C−H and π units, with a very small electrostatic contribution.[18] Moreover, the directionality of C−H/π interaction is very weak compared to that of conventional hydrogen bonds.[13] All of these lead them to conclude that the nature of CH/π interaction is significantly different from that of conventional hydrogen bonds.

Catechol (1,2-dihydroxybenzene) can be considered as an interesting system for studying stacking interactions because of several reasons: (i) its solid structure (Figure 1a) contains both $\pi-\pi$ and C−H/π interactions, (ii) each of the different dimers that can be extracted from the crystal structure contain only one of these kinds of interactions (parallel offset dimer and T-shaped dimer, Figure 1), whereas the tetramer includes both kinds, (iii) C_i symmetry of the parallel offset dimer precludes charge transfer (CT), (iv) the traditionally assumed intramolecular hydrogen bond (IHB) between hydroxyls of catechol is not related to any bond path;[19] thus, it cannot be predicted if weaker interactions like $\pi-\pi$ and C−H/π will be represented by bond paths in these systems, and (v) Its crystal structure was experimentally determined and is available in the Cambridge Crystallographic Database Center (CCDC).[20]

In this manuscript, the results obtained from the electron density analysis of catechol tetramer and dimers using the quantum theory of atoms in molecules (QTAIM)[21,22] are discussed in order to provide further understanding on the electronic rearrangements involved in $\pi-\pi$ stacking and C−H/π interactions and their possible cooperative effects in tetramers.

Computational Details. The geometry described for the catechol crystal[20] leads us to study the following systems: tetramer, **T**, parallel "offset" dimer, $\mathbf{D_1}$, orthogonal dimer, $\mathbf{D_2}$ (Figure 1), and monomer, **M**. Electronic energy, E, and electron density distribution, $\rho(\mathbf{r})$, for these systems were computed in diverse geometries: that of the crystal (C) and those obtained after complete optimization for each of them (T, D_1, D_2, M). Thus, in what follows, the concrete structures are denoted indicating the system in boldface followed by the geometry in parentheses. Two different situations can be distinguished for the monomers in $\mathbf{D_2}$ (Figure 1), $\mathbf{M^A}$(X) and $\mathbf{M^B}$(X) (X = D_2, T, or C). Superscript index A represents the monomer which is formally acting as H-donor (acid), whereas B corresponds to the H-acceptor one (base). Because $\mathbf{D_1}$ possess C_i symmetry, the monomers display a common geometry in this dimer, hereafter referred also as $\mathbf{M^A}(D_1)$, as it corresponds to real $\mathbf{M^A}$ monomers in the crystal geometry, although it does not play an acid role in $\mathbf{D_1}$.

Single-point calculations with the Truhlar's DFT functional MPW1B95[23] were carried out using the 6-311++G(2d,2p) 6d basis set with Gaussian 03 program[24] for all the systems considered in the geometry of the crystal: **T**(C), $\mathbf{D_1}$(C), $\mathbf{D_2}$(C),

* Corresponding author. E-mail: mosquera@uvigo.es.

10.1021/jp906045f CCC: $40.75
Published on Web 09/17/2009

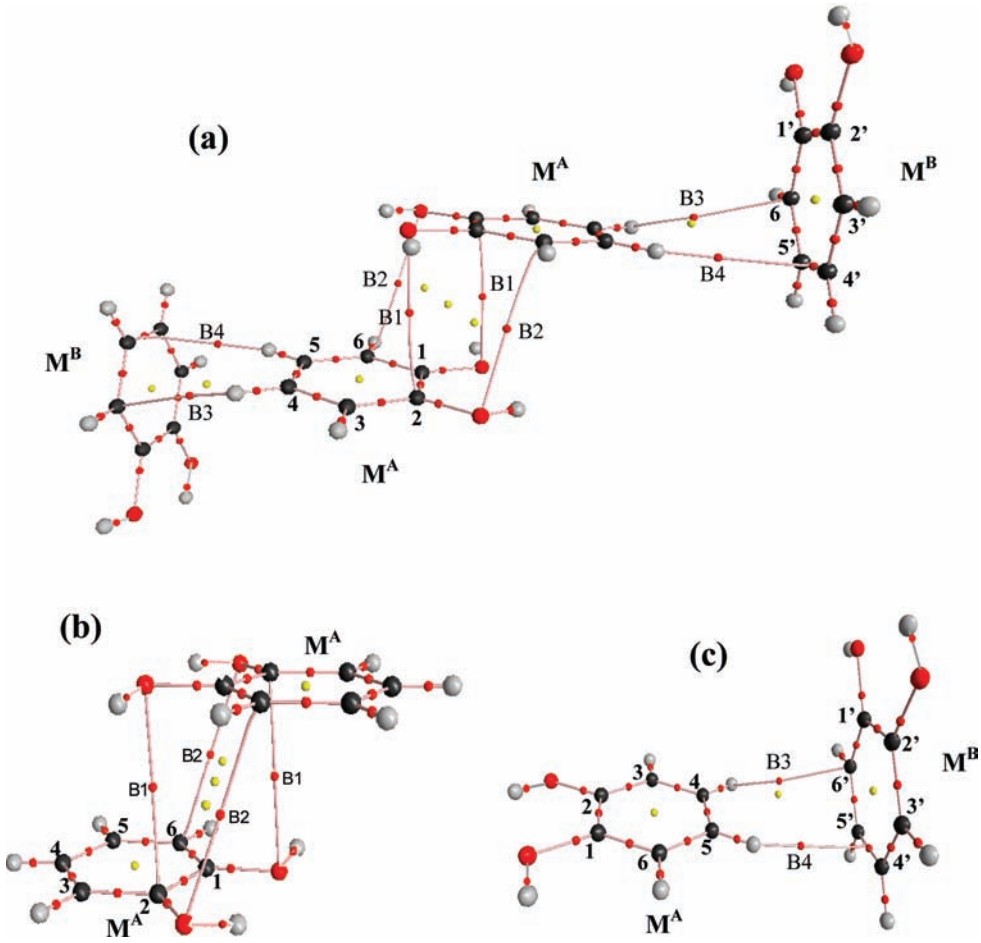

Figure 1. Molecular graphs (obtained with AIM2000 (ref 28)) indicating atom numbering and nomenclature for monomers and intermolecular bond critical points (BCPs) of tetramer **T** (a), face-to-face dimer $\mathbf{D_1}$ (b), and C−H/π dimer $\mathbf{D_2}$ (c) of catechol. Also indicated is the crystal structure data: monoclinic, $a = 9.732$, $b = 5.620$, $c = 10.332$ Å, $\beta = 114.24°$, $Z = 4$, $D = 1.419$; space group $P2_1/n$.

$\mathbf{M^A}$(C), and $\mathbf{M^B}$(C). Even although the structure in the crystal does not necessary correspond to the lowest-energy arrangements in the gas phase, as happens to benzene dimer,[25] it will work as a good estimation for the purpose of this work. In fact, we are mainly concerned with the electron density rearrangement involved in these weak interactions and not with nuclear relaxation. Thus, our electron density based interpretation is more related to binding energy, $\Delta^b E$, than to deformation energies, $\Delta^d E$. Nevertheless, aiming to obtain complexation energies in the gas phase, $\Delta^c E$, we have also computed fully optimized geometries at the same level for $\mathbf{D_1}$, $\mathbf{D_2}$, **T**, and **M**, labeled, respectively, $\mathbf{D_1}(D_1)$, $\mathbf{D_2}(D_2)$, **T**(T), and **M**(M). Moreover, we have also carried out single-point calculations for $\mathbf{M^A}$ and $\mathbf{M^B}$ in the geometries they display in optimized dimers and tetramer, which allow to obtain deformation energies.

Comparison of $\rho(\mathbf{r})$ obtained for a certain complex, $\rho^C(\mathbf{r})$, and the summation of those computed for its constituting fragments, $\rho^i(\mathbf{r})$, ($i = \mathbf{M^A}$, $\mathbf{M^B}$), is provided through electron deformation density, $\Delta\rho(\mathbf{r})$, plots (eq 1).

$$\Delta\rho(\mathbf{r}) = \rho^C(\mathbf{r}) - \sum_i \rho^i(\mathbf{r}) \qquad (1)$$

Counterpoise correction for basis set superposition error was not performed so that MPW1B95 functional was developed in such a way that they give reasonable results for noncovalent interactions both with and without counterpoise corrections, and the developers pointed out that they should be usable without the need of counterpoise corrections, especially when the basis is triple-ζ quality or better (as it is here).[26]

In each molecule, the QTAIM charge density analysis was performed with the AIMPAC[27] package of programs and AIM2000.[28] In this work we focus on the properties at the bond critical points (BCP) of $\rho(\mathbf{r})$:[21,22] electron density, $\rho(\mathbf{r}_c)$, its laplacian, $\nabla^2\rho(\mathbf{r}_c)$, and the value of the total energy density, $H(\mathbf{r}_c)$. We also discuss some of the atomic properties provided by integrating $\rho(\mathbf{r})$ over atomic basins: atomic electron population, $N(\Omega)$, atomic energy, $E(\Omega)$, the integrated value of the $L(\mathbf{r})$ function, $L(\Omega)$, which should be zero for a perfectly determined basin; the first vectorial moment of the atomic electron density, $\mu(\Omega)$, with its module and components; the first and second scalar moments of $\rho(\mathbf{r})$, $r^1(\Omega)$ and $r^2(\Omega)$, atomic volumes computed making use of 10^{-3} au, $v_1(\Omega)$, and 2×10^{-3} au, $v_2(\Omega)$, and the corresponding electron populations enclosed by them, $N_1(\Omega)$ and $N_2(\Omega)$, the elements of the matrix of the atomic electron quadrupole moment, $Q_{ij}(\Omega)$, especially $Q_{zz}(\Omega)$ where z represents an axis that is orthogonal to the ring of $\mathbf{M^A}$ monomer, and finally, the atomic Shannon entropy of the electron distribution, $Sh(\Omega)$.

The accuracy obtained in the determination of the integrated properties was checked using standard criteria. Thus, summations of $N(\Omega)$ and atomic energy, $E(\Omega)$, values for each molecule reproduce total electron populations and electronic molecular energies within 2×10^{-4} au and 2.5 kJ mol^{-1},

TABLE 1: Total MPW1B95′6-311++G(2d,2p) 6d Electronic Molecular Energies (in au) and MP2/6-311++G(2d,2p) 6d Zero-Point Vibrational Energy (ZPVE) and Thermal Corrections to Energy (TCE) at 298.15 K (in au) for the Systems Here Studied in Diverse Geometries

geometry	$\mathbf{M^A}$	$\mathbf{M^B}$	**M**	$\mathbf{D_1}$	$\mathbf{D_2}$	**T**
C	−382.60259	−382.60227		−765.20957	−765.20635	−1530.41842
T	−382.65560	−382.65783				
D_1	−382.65589					
D_2	−382.65786	−382.65778				
optimized			−382.65795	−765.32683	−765.31905	−1530.64948
ZPVE			0.10900	0.21831	0.21860	
TCE			0.116791	0.23448	0.23578	

TABLE 2: Complexation Energies, $\Delta^c E$, for Dimers D_1 and D_2 and Binding, $\Delta^b E$, and Deformation Energies of Monomers, $\Delta^d E$, in Diverse Geometries, for All the Systems Here Studied[a]

	(**T**)	(**C**)	($\mathbf{D_1}$)	($\mathbf{D_2}$)
$\Delta^c E$			−19.6	−1.2
$\Delta^b E[\mathbf{D_1}]$		−11.5	−39.5	
$\Delta^b E[\mathbf{D_2}]$		−3.9		−9.0
$\Delta^b E[\mathbf{T}]$	−59.4	−22.8		
$\Delta^d E[\mathbf{M^A}]$	6.2	145.3	5.4	0.2
$\Delta^d E[\mathbf{M^B}]$	0.3	146.2		0.4

[a] All values in kJ mol^{-1}.

respectively. No atom was integrated with absolute values of $L(\Omega)$[21,22] larger than 2×10^{-3} au.

Results and Discussion

Face-to-Face Dimer ($\mathbf{D_1}$). Molecular energies computed at the MPW1B95/6-311++G(2d,2p) 6d level for this dimer and its monomer in the crystal geometry, as well as for the corresponding completely optimized structures, and for the monomer in the geometry of the optimized dimer are shown in Table 1. It has to be noticed that MPW1B95/6-311++G(2d,2p) 6d frequencies cannot be computed in Gaussian-03 making use of the same command line where optimization is requested. In fact, this leads to artifacts resulting in several imaginary frequencies. To get around of this problem geometry optimization and frequency calculation should be performed independently. Using this procedure all the frequencies computed for all optimized geometries here studied are real. We also performed MP2/6-311++G(d,p) optimizations, whose final geometries were confirmed as true minima by vibrational analysis. Nonetheless, being aware that MP2 calculations usually overestimate stacking energies,[29] we are not using these energies. **M**(M) geometries obtained with both computational levels for the monomer differ by less than 0.017 Å (bond lengths), and 1.4° (bond angles). The only noticeable variation is the nonplanarity of MP2 H−O−C−C dihedral angles (up to 19.7°). Moreover, the planar structure was not found as a minimum on the MP2 hypersurface after several attempts. Zero-point vibrational energy (ZPVE) and thermal corrections to energy (TCE) were computed using MPW1B95/6-311++G(2d,2p) frequencies in all cases.

Results obtained (Table 2) show that dimer $\mathbf{D_1}$ is the most stable one, both comparing optimized structures (by 18.5 kJ mol^{-1}) and crystal geometries (30.6 kJ mol^{-1}) for dimers $\mathbf{D_1}$ and $\mathbf{D_2}$. Also, we obtain −19.6 kJ mol^{-1} for the complexation energy of isolated $\mathbf{D_1}$. Deformation energies indicate each monomer is being destabilized by 5.4 kJ mol^{-1} in the geometry of the $\mathbf{D_1}$ isolated dimer, $\mathbf{D_1}$(D_1), and by 145.3 kJ mol^{-1} in its geometry in the crystal, $\mathbf{D_1}$(C). Binding energies of −11.5 and −39.5 kJ mol^{-1} were obtained using, respectively, crystal and optimized dimer geometries.

$\mathbf{D_1}$ displays four intermolecular bond paths (Figure 1b), which by symmetry can be reduced to two different interactions: C2···O1 and O2···C6. In contrast, the C−H/π dimer $\mathbf{D_2}$ only presents two intermolecular bond paths (Figure 1c): C4−H···C6′ and C5−H···C5′. Considering the similarity among all the $\rho(\mathbf{r}_c)$ values (Table 3), the larger number of bond paths can be invoked to justify the preference for $\mathbf{D_1}$. Values of all the BCP properties associated to $\pi-\pi$ interactions are very small: $\rho(\mathbf{r}_c)$ values are between 4×10^{-3} and 6×10^{-3} au; $\nabla^2\rho(\mathbf{r}_c)$ ones are positive and between 14×10^{-3} and 21×10^{-3} au. Also $H(\mathbf{r}_c)$ values are positive, between 7.2×10^{-4} and 9.2×10^{-4} au. They are similar to those found in previous QTAIM works on stacking interactions in DNA bases.[30] On the other hand, this complexation does not alter BCP properties computed for the monomers in the same geometry, whose $\rho(\mathbf{r}_c)$ values are kept within 0.002 au.

Atomic properties of the optimized catechol monomer, **M**(M), are altered significantly in $\mathbf{D_1}$(C). Hence, we observe four $\Delta N(\Omega)$ variations exceeding of 0.09 au: C5, C4, C6, and H5. Surprisingly, most of these atoms are not involved in stacking bond paths and even C4 is the atom placed furthest away from them. To analyze these variations we have also computed QTAIM integrated properties for $\mathbf{M^A}$(C). It is remarkable that for some properties, like $N(\Omega)$, the variations due to geometry deformation, $\Delta^d N(\Omega)$ (those observed from **M**(M) to $\mathbf{M^A}$(C)), are significantly larger than those of binding through stacking interaction, $\Delta^b N(\Omega)$ (those observed between $\mathbf{D_1}$(C) and $\mathbf{M^A}$(C)) (Table 4). In fact, the rms of $\Delta^d N(\Omega)$ is 0.066 au and that of $\Delta^b N(\Omega)$ is only 0.007 au. On the contrary, properties related to electron density polarization, like $\mu_z(\Omega)$ and $Q_{zz}(\Omega)$, experience larger variations because of binding than due to geometry deformation. Thus, the rms of $\Delta^d\mu_z(\Omega)$ is 0.017 au and the rms of $\Delta^b\mu_z(\Omega)$ is 0.033 au, and the rms of $\Delta^d Q_{zz}(\Omega)$ is 0.064 au, whereas that of $\Delta^b Q_{zz}(\Omega)$ is 0.097 au.

If we concentrate on Δ^b variations, the summations of property variations (Table 5) along a monomer (i) confirm there is no global CT between monomers ($\sum \Delta^b N(\Omega) = 0$), (ii) indicate there is a slight global polarization which moves the center of $\rho(\mathbf{r})$ away from the intermolecular region ($\sum\Delta^b\mu_z(\Omega) = -62.10^{-3}$ au), and (iii) show that, globally, $\rho(\mathbf{r})$ flattens with regard to an axis orthogonal to the molecular plane of catechol ($\sum\Delta^b Q_{zz}(\Omega) = 0.818$ au). In general, the largest variations (in absolute value) correspond to atoms involved in stacking bond paths (O1, O2, C2, and C6) or closely placed to them. So, the largest $|\Delta^b N(\Omega)|$, $|\Delta^b\mu_z(\Omega)|$, and $|\Delta^b Q_{zz}(\Omega)|$ values are, respectively, shown by O2, C2, and C6 (Table 4 and Figure 2). Although there is no straightforward trend and interpretation for the sign of $\Delta^b N(\Omega)$ and $\Delta^b\mu_z(\Omega)$, $\Delta^b Q_{zz}(\Omega)$ is positive for all the atoms displaying a significant variation ($|\Delta^b Q_{zz}(\Omega)| > 0.01$ au). This means binding stacking interactions flatten $\rho(\mathbf{r})$ toward the molecular plane of catechol around all those atoms where $\Delta^b Q_{zz}(\Omega) < 0$.

TABLE 3: Main Properties (in au) of the Intermolecular BCPs (Figure 1) Found for the D_1(C), D_2(C), and T(C) of Catechol[a]

interaction	BCP	R	**D**(C) $10^3\rho(\mathbf{r}_c)$	**T**(C) $10^3\rho(\mathbf{r}_c)$	**D**(C) $10^3\nabla^2\rho(\mathbf{r}_c)$	**T**(C) $10^3\nabla^2\rho(\mathbf{r}_c)$	**D**(C) $10^4H(\mathbf{r}_c)$	**T**(C) $10^4H(\mathbf{r}_c)$
$\pi-\pi$	B1	3.429	4.39	4.37	14.56	14.60	7.20	7.30
	B2	3.272	5.96	5.97	21.17	21.22	9.20	9.40
C−H/π	B3	3.091	3.58	3.56	11.48	11.50	6.60	6.60
	B4	2.831	6.31	6.31	20.21	20.21	9.50	9.50

[a] Internuclear distances, R, in angstroms.

TABLE 4: Variations in the Electron Population by Deformation Geometries upon D_1(C) Formation (All in au Values Multiplied by 10^3)

	$\Delta^cN(\Omega)$ in $\mathbf{D_1}$(C)	$\Delta^dN(\Omega)$ in $\mathbf{M^A}$(C)	$\Delta^bN(\Omega)$ in $\mathbf{D_1}$(C)
C1	0	9	−9
C2	42	39	3
C3	−63	−64	1
C4	−91	−86	−5
C5	−106	−105	0
C6	−91	−85	−6
H1	−44	−40	−4
H2	−44	−39	−4
H3	63	53	11
H4	87	83	4
H5	100	98	2
H6	68	77	−9
O1	35	31	4
O2	46	31	15

This flattening can be also inferred from the variations in the scalar moments of $\rho(\mathbf{r})$, whose summations, $\sum\Delta^br^1(\Omega)$ and $\sum\Delta^br^2(\Omega)$, are negative (Table 5), indicating $\rho(\mathbf{r})$ approaches, in average, the nucleus of basins and turns into a more spherical distribution after complex formation. Variations experienced upon binding by atomic volumes $v_1(\Omega)$ and $v_2(\Omega)$ and by the electron population enclosed by them indicate this $\rho(\mathbf{r})$ flattening affects mainly the diffuse electron density distributed far from the nuclei. Accordingly, $\sum\Delta^bv_1(\Omega)$ is negative and $\sum\Delta^bv_2(\Omega)$ positive, showing the volume occupied by the electron density between 2×10^{-3} and 1×10^{-3} au has decreased upon stacking. At the same time $\sum\Delta^bN_1(\Omega)$ is exceeded by $\sum\Delta^bN_2(\Omega)$, so the electron population enclosed in $\mathbf{M^A}$(C) by 2×10^{-3} and 1×10^{-3} au isosurfaces, $\sum\Delta^bN_{12}(\Omega)$, has also decreased upon stacking. Furthermore, decrease of diffuse electron density is also pointed out by the depletion of $Sh(\Omega)$ (Table 5). $Sh(\Omega)$ depletions are specially important in those atoms involved in intermolecular bond paths. Figure 3 shows that atoms experiencing significant depletions of $Q_{zz}(\Omega)$ display important negative $\Delta^bSh(\Omega)$ values, indicating $\Delta^bQ_{zz}(\Omega)$ acts for them as the main origin for the relative increase in the uniformity of $\rho(\mathbf{r})$ affecting $\mathbf{M^A}$ upon stacking interaction with another $\mathbf{M^A}$ monomer to form $\mathbf{D_1}$.

$\Delta^bN(\Omega)$ values are in close relation to $\Delta\rho(\mathbf{r})$ (Figure 2a). The small variations observed for the former agree with the small magnitude achieved by the latter. Thus, we have to choose very low isosurfaces (below 0.001 au in absolute value) to obtain meaningful regions for $\Delta\rho(\mathbf{r})$. We observe that there are enhancement and depletion regions around all the atoms involved in bond paths. Thus, in agreement with the description provided by $\Delta^bN(\Omega)$, $\Delta^b\mu_z(\Omega)$, and $\Delta^bQ_{zz}(\Omega)$ values, the alteration of $\rho(\mathbf{r})$ upon stacking interactions is more related to the distortion of electron distributions in atomic basins than to transfer of electron density from one basin to another. Most of the enhanced $\rho(\mathbf{r})$ regions are in the molecular plane around oxygen atoms, C2, and C1−O1, and C6−H6 bonds. All of these regions are close to depletion ones, placed out of the plane (at both sides) and not far from it. This general situation reverses for C3, where $\rho(\mathbf{r})$ is enlarged outside the molecular plane, whereas it diminishes in the central part of C3−H3 bond. Finally, small depletion areas are observed around hydroxyl oxygens. Overall, all areas where $\Delta\rho(\mathbf{r})$ is significant do not correspond to the region where monomers, delimited according to a certain $\rho(\mathbf{r})$ isosurface, e.g., 10^{-3} au, overlap. This overlap is computed as 19.1 au in $\mathbf{D_1}$(C) when using 10^{-3} au delimiting isosurfaces.

The reliability of Mulliken's overlap and orientation principle has been checked comparing the zones of maximum highest occupied molecular orbital/lowest unoccupied molecular orbital (HOMO/LUMO) overlap between monomers with the set of intermolecular bond paths. As has been found in quinhydrone complex,[9] the whole set of intermolecular bond paths displayed by the stacking complex $\mathbf{D_1}$ can be explained by the overlap between the HOMO and LUMO of $\mathbf{M^A}$ monomers (Figure 4, top). Nevertheless, it has to be noticed that O2···C6 bond paths are only explainable by this principle considering the overlap between the HOMO on O2 and the LUMO on C6, as the latter atom has no significant contribution to the HOMO. This could lead to expect a positive value for Δ^bN(C6). In contrast, we have found a negative value for this quantity (Table 4) that can be explained assuming HOMO−LUMO transferences are accompanied by $\rho(\mathbf{r})$ reorganization among the atoms of each monomer, as was previously proposed for quinhidrone complex.[9]

C−H/π Dimer (D_2). As above indicated this dimer is less stable than $\mathbf{D_1}$ both if stability is measured through Δ^cE or Δ^bE values; the latter referred either to crystal or optimized geometries (Table 2). In contrast, deformation energies are much smaller in $\mathbf{D_2}$ for both monomers. Binding energies of −3.9 and −9.0 kJ mol^{-1} were obtained using, respectively, crystal and optimized dimer geometries.

The two intermolecular bond paths present in $\mathbf{D_2}$ display similar $\rho(\mathbf{r}_c)$, $\nabla^2\rho(\mathbf{r}_c)$, and $H(\mathbf{r}_c)$ values to those of $\pi-\pi$ interactions in $\mathbf{D_1}$ (Table 3). Nevertheless, we notice that the closest pairs of values (e.g., sets of B2 and B4 values, or sets of B1 and B3 values in Table 3) are obtained when the C−H/π interaction distance is around 0.4 Å shorter than the corresponding $\pi-\pi$ one. As $\rho(\mathbf{r}_c)$ values are known to depend strongly with interatomic distances, decreasing when interatomic distances are longer,[31] we could infer that $\pi-\pi$ interactions are stronger than C−H/π ones if they take place for the same interatomic distance. BCP properties for C−H/π bond paths are in the range of those previously reported for C−H···O IHB ($\rho(\mathbf{r}_c)$ is 3.9×10^{-3} au and $\nabla^2\rho(\mathbf{r}_c)$ is 16.0 au for this IHB in benzene−formaldehyde complex,[32] and $\rho(\mathbf{r}_c)$ and $\nabla^2\rho(\mathbf{r}_c)$ are, respectively, between 0.9×10^{-3} and 5.0×10^{-3} au and between 4.2×10^{-3} and 17.0×10^{-3} au in the set of IHBs present in the dimers of dimethoxymethane[33]). They are also in the range displayed by the IHBs established between complexes like HCl−HF or H_3P−HF.[34] Again, this complexation does not alter BCP properties of the monomers ($\rho(\mathbf{r}_c)$ values are kept within 0.002 au and $\nabla^2\rho(\mathbf{r}_c)$ within 0.003 au).

In contrast with symmetric dimer $\mathbf{D_1}$, where there is no CT, the formation of $\mathbf{D_2}$(C) takes place with a non-negligible CT

TABLE 5: Variations Experienced by Selected Integrated Properties during D_1(C), D_2(C), and T(C) Formation of Catechol Monomers (Figure 1) (All Values in au Multiplied by 10^3)

	unit	$\sum\Delta^b N(\Omega)$	$\sum\Delta^b N(\Omega^*)^a$	$\sum\Delta^b r^1(\Omega)$	$\sum\Delta^b r^2(\Omega)$	$\sum\Delta^b Sh(\Omega)$	$\sum\Delta^b \upsilon_1(\Omega)$	$\sum\Delta^b \upsilon_2(\Omega)$	$\sum\Delta^b N_1(\Omega)$	$\sum\Delta^b N_2(\Omega)$	$\sum\Delta^b N_{12}(\Omega)$
$\mathbf{D_1}$(C)	$\mathbf{M^A}$(C)	0	5	−63	−467	−57	−9.6	7.4	44	68	−25
$\mathbf{D_2}$(C)	$\mathbf{M^A}$(C)	11	−15	19	19	−49	2.2	7.4	35	42	−7
	$\mathbf{M^B}$(C)	−11	−6	−61	−353	−36	−4.8	4.0	17	29	−12
T(C)	$\mathbf{M^A}$(C)	11	−13	−53	−527	−112	−8.0	14.3	78	109	−31
	$\mathbf{M^B}$(C)	−11	5	−66	−382	−38	−4.9	3.8	16	28	−12

[a] Ω* refers to atoms connected through intermolecular bond paths.

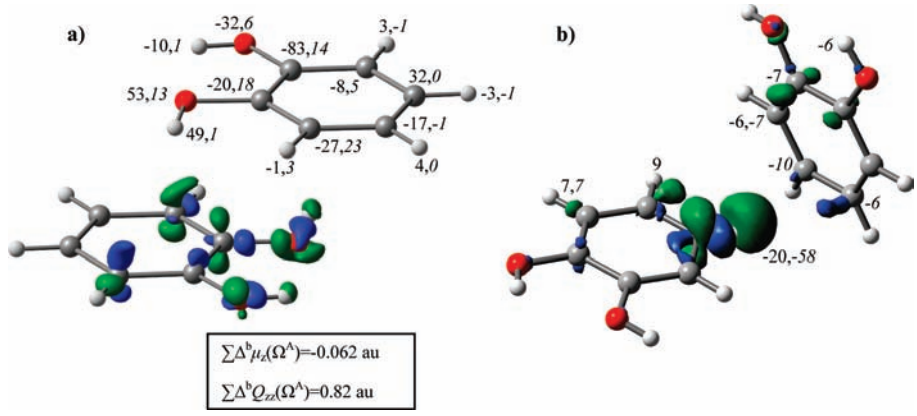

Figure 2. Deformation density plots for $\mathbf{D_1}$(C) and $\mathbf{D_2}$(C) (a and b, respectively). Blue and green denote, respectively, 4×10^{-4} au and -4×10^{-4} au isosurfaces. $\Delta^b\mu_z(\Omega)$ and $\Delta^b Q_{zz}(\Omega)$ (in italics) values (in au multiplied by 10^3 for the former and 10^2 for the latter) are shown for $\mathbf{D_1}$(C), whereas $\Delta^b N(\Omega)$ and $\Delta^b Sh(\Omega)$ (in italics) are shown (both in au multiplied by 10^3) for $\mathbf{D_2}$(C). Only $|\Delta^b Sh(\Omega)| \geq 5 \times 10^{-3}$ au are shown.

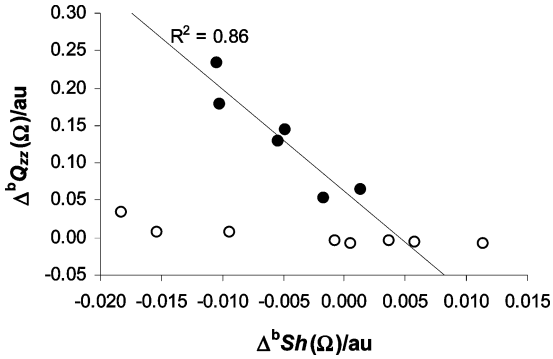

Figure 3. Plot of $\Delta^b Q_{zz}(\Omega)$ vs $\Delta^b Sh(\Omega)$ for $\mathbf{D_1}$(C). Atoms experiencing significant changes of $Q_{zz}(\Omega)$ are shown in closed face and those with negligible variations (up to ± 0.03 au) in open face.

and 0.011 au are transferred from $\mathbf{M^B}$(C) to $\mathbf{M^A}$(C). This keeps in line with previous descriptions of CT due of IHB in complexes with nonsymmetric geometries, where electron density is transferred from the base ($\mathbf{M^B}$ in this case) to the acid. For instance, Koch and Popelier reported CT from 0.005 au in N_2−HF complex to 0.046 au in NH_3−HF complex.[32]

As a consequence of binding, H-acceptor $\mathbf{M^B}$(C) destabilizes ($\sum\Delta^b E(\Omega) = 7.9$ kJ mol^{-1}) in a lower extent than the stabilization gained by H-donor $\mathbf{M^A}$(C) ($\sum\Delta^b E(\Omega) = -10.1$ kJ mol^{-1}), which is also larger than that gained by each $\mathbf{M^A}$(C) unit during the formation of $\mathbf{D_1}$(C) ($\sum\Delta^b E(\Omega) = -9.7$ kJ mol^{-1}).

The analysis of $\Delta^b N(\Omega)$ values computed for $\mathbf{D_2}$(C) shows that the largest variations correspond to atoms involved in intermolecular bond paths (IBPs) (H4, H5, C5′, and C6′), C1′, and C3 (Figure 2b). The electron density lost by the hydrogen in the C−H/π bond path with the highest $\rho(\mathbf{r}_c)$ ($\Delta^b N$(H5) = −0.020 au) is quite similar to that computed for C−H···O bonds in the complex between acetone and CH_3CHCl_2 (−0.024 au)[32] and not far from those obtained for a series of O−H···O intermolecular hydrogen bonds between water and diverse oxygen-containing bases (−0.028 to −0.036 au).[35] On the contrary, $\Delta^b N$(H4) is positive. Nonetheless, it should be considered that H4 is connected to C6′ through the weakest IBP, which therefore have not been established in optimum conditions but conditioned by the formation of the strongest one (H5···C5′). In addition, enhancements of H-donor electron population upon IHB formation have been previously reported by Rozas et al. for systems displaying inverse IHB[36] and by Vila and Mosquera for so simple complexes as H_2S−HF, H_3N−HF, or H_3P−HF where the electron population of H-donor basin is increased by 0.022, 0.011, and 0.028 au, respectively.[37]

For this dimer we do not report $\Delta^b Q_{zz}(\Omega)$ and $\Delta^b\mu_z(\Omega)$ values because both monomers are not sharing a common axis. Therefore, we analyze electron density reorganization using $\Delta^b Sh(\Omega)$ values, which display a rough linear correlation with $\Delta^b Q_{zz}(\Omega)$ ones when the latter are significant, as illustrated by Figure 3 for dimer $\mathbf{D_1}$. In this case, we notice that H5 (donor hydrogen) is the only atom of the acid monomer ($\mathbf{M^A}$) displaying a non-negligible $\Delta^b Sh(\Omega)$ value (Figure 2b), evidencing the localized character of this C−H/π interaction, in contrast to what happens in $\mathbf{D_1}$, affected by $\pi-\pi$ interaction. Overall, $\sum\Delta^b Sh(\Omega)$ values indicate $\rho(\mathbf{r})$ becomes more uniform in both monomers upon binding (Table 4). Another different trend (referring to those observed in $\mathbf{D_1}$) is found for $\sum\Delta^b r^1(\Omega)$ and $\sum\Delta^b r^2(\Omega)$. They are negative for the base monomer $\mathbf{M^B}$ and slightly positive for $\mathbf{M^A}$ (Table 4). Hence, $\rho(\mathbf{r})$ only flattens for $\mathbf{M^B}$. This is also the only monomer where we observe the volume occupied by the electron density between 2×10^{-3} and 1×10^{-3} au has decreased upon binding ($\sum\Delta^b \upsilon_1(\Omega) < 0$ and $\sum\Delta^b \upsilon_2(\Omega) > 0$), which is not true for the H-donor monomer. This can be interpreted as that $\mathbf{M^B}$ participates in the bonding as a global system, while the local character of this interaction in $\mathbf{M^A}$ has been already evidenced by $\Delta^b Sh(\Omega)$ values. In the same vein, we also notice the presence of four non-negligible $\Delta^b Sh(\Omega)$ values in $\mathbf{M^B}$ (Figure 2b).

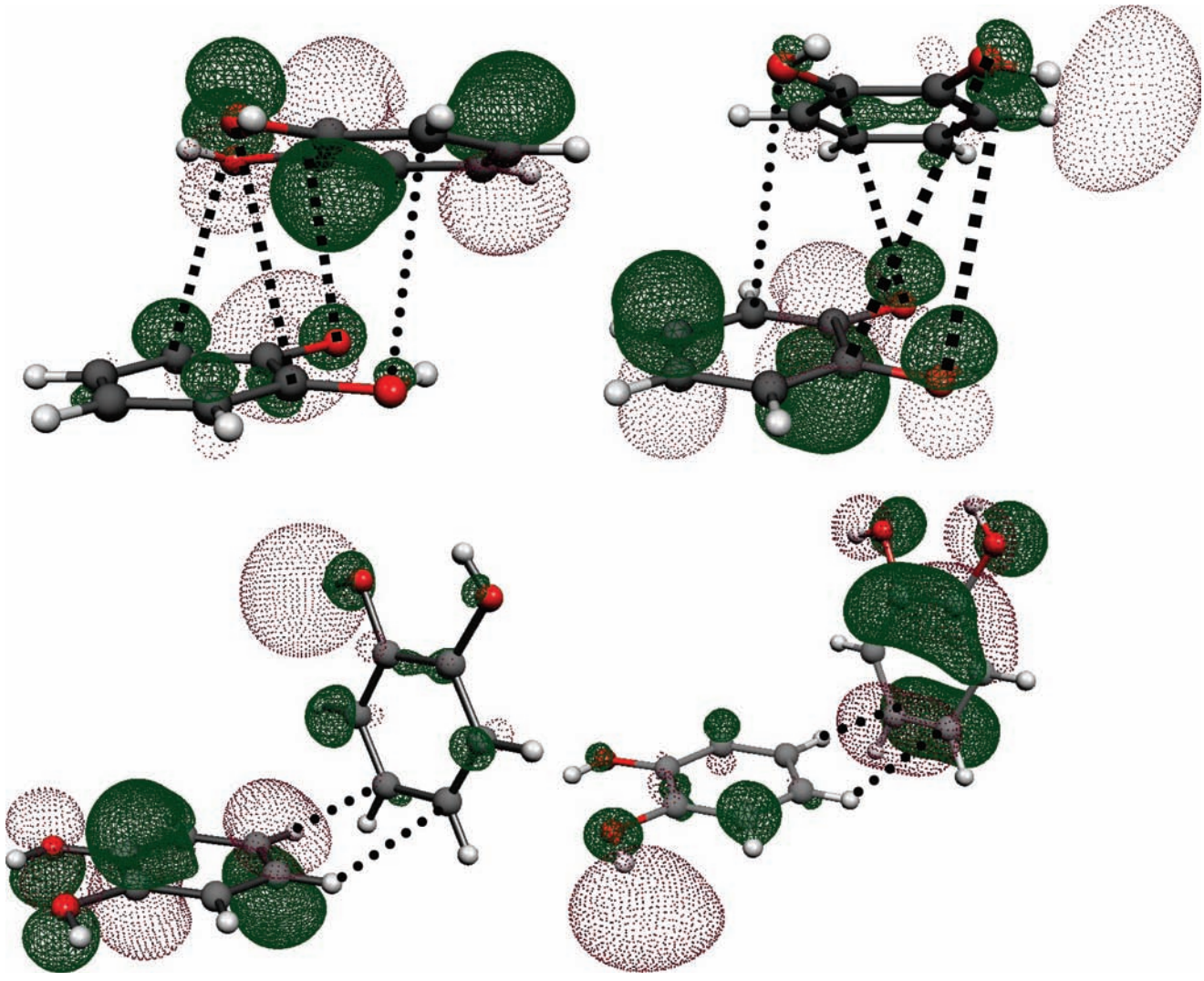

Figure 4. Plots of ±0.04 au isosurfaces for the HOMO and LUMO of $\mathbf{M^A}$ monomers in $\mathbf{D_1}$ (top) and $\mathbf{M^A}$ and $\mathbf{M^B}$ monomers in $\mathbf{D_2}$ (bottom). Drawings on the left show the LUMO in the lower monomer and the HOMO in the upper one (in the top part) and the LUMO in $\mathbf{M^B}$ and the HOMO in $\mathbf{M^A}$ (in the bottom part). Drawings on the right show, in both dimers, the opposite cases. Dotted lines indicate the atom connected by intermolecular bond paths (Figure 1). ●●● and ■■■ represent, respectively, bond paths that are explainable and not explainable by HOMO/LUMO overlap.

The $\Delta\rho(\mathbf{r})$ plot for this dimer (Figure 2b) is also rather different from that of $\mathbf{D_1}$. In this case the deformation concentrates on the strongest IBP, which displays alternate depletion and enhancement regions, each of them resembling a certain cylindrical symmetry, typical of IHBs, contrasting again with the picture observed for $\pi-\pi$ interactions in $\mathbf{D_1}$ (Figure 2a). We also notice the effects of C−H/π interactions are localized in $\mathbf{M^A}$ but more delocalized in $\mathbf{M^B}$.

In this dimer, HOMO/LUMO overlap between monomers cannot be invoked to explain the set of IBPs (Figure 4, bottom), as both the HOMO and LUMO have negligible contribution from hydrogens involved in C−H/π interactions.

Tetramer (T). $\Delta^b E$ values of −22.8 and −59.4 kJ mol^{-1} were computed for **T**(C) and **T**(T), respectively, from MPW1B95/6-311++G(2d,2p) 6d energies. Intermolecular interactions among tetramers in the crystal reduce binding energy by 36.5 kJ mol^{-1} and increase the summation of deformation energies of monomers by 570 kJ mol^{-1}. In fact, deformation energies for monomers are 6.2 kJ mol^{-1}, $\mathbf{M^A}$, and 0.3 kJ mol^{-1}, $\mathbf{M^B}$, in **T**(T), and, respectively, 145.3 and 146.2 kJ mol^{-1} in **T**(C). We also notice that cooperative effects contribute to stabilize the tetramer by −3.5 kJ mol^{-1} in **T**(C) and by −2.0 kJ mol^{-1} in the optimized **T**(T) structure.

In agreement with this small contribution of cooperative effects to binding energy, the molecular graph of the tetramer is just the superposition of those obtained for both dimers (Figure 1), showing eight IBPs. Four of them correspond to C−H/π interactions between each pair of orthogonal catechol monomers and four to the C···O bond paths described above for dimer $\mathbf{D_1}$. Table 2 shows that differences between BCP properties in corresponding critical points of dimers and tetramer are below 2×10^{-5} au for $\rho(\mathbf{r}_c)$, 5×10^{-5} au for $\nabla^2\rho(\mathbf{r}_c)$, and 2×10^{-5} au for $H(\mathbf{r}_c)$. Thus, cooperative effects between $\pi-\pi$ and C−H/π interactions on BCP properties in **T**(C) can be considered negligible.

CT remains the same in each C−H/π unit of the tetramer. That is, the population of each $\mathbf{M^A}$ unit increases 0.011 au in the tetramer with regard to that of the isolated monomer in the same geometry, whereas those of $\mathbf{M^B}$ units are reduced in the same amount, and no cooperative effects are noticeable for the whole electron density of monomers. Atomic properties computed for $\mathbf{M^A}$(C), $\mathbf{M^B}$(C), $\mathbf{D_1}$(C), $\mathbf{D_2}$(C), and **T**(C) allow us to obtain cooperative effects on them in the crystal geometry. For the sake of simplicity, we have restricted ourselves to analyze cooperative effects on $\Delta^b N(\Omega)$ and $\Delta^b E(\Omega)$, denoted as $\Delta^{cb} N(\Omega)$ and $\Delta^{cb} E(\Omega)$, bearing in mind the interactions

TABLE 6: Atomic Electron Populations of the Monomers, M^A and M^B, in the Systems Considering Crystal Geometry $D_1(C)$, $D_2(C)$, T(C), and Cooperative Effects Due to Tetramer Formation on the Atomic Electron Populations[a]

	$N^{T(C)}(\Omega)$	$N^{D1(C)}(\Omega)$	$N^{D2(C)}(\Omega)$	$N^{M(C)}(\Omega)$	$\Delta^{cb}N(\Omega)$
			M^A		
C1	5.5074	5.5064	5.5173	5.5173	−0.0005
C2	5.4903	5.4892	5.4903	5.4903	−0.0026
C3	5.9421	5.9361	5.9353	5.9353	0.0059
C4	5.9217	5.9150	5.9166	5.9166	0.0100
C5	5.9093	5.9017	5.9061	5.9061	0.0037
C6	5.9227	5.9208	5.9236	5.9236	0.0052
H1	0.3597	0.3586	0.3624	0.3624	0.0017
H2	0.3470	0.3460	0.3501	0.3501	0.0010
H3	1.0288	1.0256	1.0223	1.0223	−0.0043
H4	1.0756	1.0706	1.0754	1.0754	−0.0041
H5	1.0617	1.0842	1.0618	1.0618	−0.0025
H6	1.0606	1.0607	1.0726	1.0726	−0.0030
O1	9.1897	9.1910	9.1914	9.1914	−0.0054
O2	9.1945	9.1953	9.1858	9.1858	−0.0059
			M^B		
C1′	5.5128		5.5092	5.5159	0.0036
C2′	5.4845		5.4867	5.4857	−0.0022
C3′	5.9364		5.9387	5.9342	−0.0023
C4′	5.9216		5.9198	5.9200	0.0018
C5′	5.9035		5.8987	5.9023	0.0049
C6′	5.9267		5.9205	5.9264	0.0062
H1′	0.3623		0.3613	0.3627	0.0010
H2′	0.3492		0.3482	0.3502	0.0010
H3′	1.0139		1.0154	1.0158	−0.0015
H4′	1.0654		1.0676	1.0665	−0.0022
H5′	1.0796		1.0816	1.0818	−0.0019
H6′	1.0692		1.0712	1.0698	−0.0020
O1′	9.1848		9.1877	9.1876	−0.0029
O2′	9.1792		9.1827	9.1815	−0.0035

[a] All values in au.

affecting each kind of monomer: C−H/π and $\pi-\pi$ for $\mathbf{M^A}$ and only C−H/π for $\mathbf{M^B}$. They are obtained with different expressions (eq 2 for $\mathbf{M^A}$ and eq 3 for $\mathbf{M^B}$), where Ω^A and Ω^B are atoms of monomers $\mathbf{M^A}$ and $\mathbf{M^B}$, and Δ^{bT}, Δ^{bD1}, and Δ^{bD2} represent, respectively, the binding variations of **T**(C), $\mathbf{D_1}$(C), and $\mathbf{D_2}$(C).

$$\Delta^{cb}N(\Omega^A) = \Delta^{bT}N(\Omega^A) - \Delta^{bD1}N(\Omega^A) - \Delta^{bD2}N(\Omega^A) \quad (2)$$

$$\Delta^{cb}N(\Omega^B) = \Delta^{bT}N(\Omega^B) - \Delta^{bD2}N(\Omega^B) \quad (3)$$

We notice that, although cooperative effects do not affect the global electron population of monomers, they are significant on some atoms (Table 6), reaching 0.010 au for C4 in $\mathbf{M^A}$ and 0.006 au for C6 in $\mathbf{M^B}$. We remark that, contrary to what could be expected, the largest $\Delta^{cb}N(\Omega)$ values do not correspond to the atoms not included in $\pi-\pi$ or C−H/π bond paths. Even we observe that, in spite of the global CT observed for C−H/π formation is the same in $\mathbf{D_2}$(C) and **T**(C), the evolution followed by $\rho(\mathbf{r})$ is different. So, the subset of atoms attached to the other monomer by IBPs, $\{\Omega^*\}$, in $\mathbf{M^B}$ goes from losing electron population in $\mathbf{D_2}$(C) to gaining it in **T**(C) as reflected by $\sum\Delta^{b}N(\Omega^*)$ values in Table 5.

It is also remarkable that $\Delta^{cb}N(\Omega)$ and $\Delta^{cb}E(\Omega)$ values are lineally correlated for each element (r^2 always above 0.91). Finally, the stabilization of $\mathbf{M^A}$ in the tetramer is −25.6 kJ mol^{-1} revealing cooperative effects ($\sum\Delta^{cb}E(\Omega) = -5.8$ kJ mol^{-1}) between the $\pi-\pi$ and C−H/π interactions affecting the same monomer. In contrast, $\mathbf{M^B}$ experiences nearly the same destabilization in dimer $\mathbf{D_2}$ as in the tetramer ($\sum\Delta^{cb}E(\Omega) < 1$ kJ mol^{-1}).

Conclusions

Face-to-face dimer ($\mathbf{D_1}$) is most stable than that due to C−H/π interactions ($\mathbf{D_2}$). The former displays four IBPs, whereas the latter only presents two. Deformation energies are significantly larger in $\mathbf{D_1}$, which is counterbalanced by a more negative binding energy. According to $\rho(\mathbf{r}_c)$ values increased binding can be only ascribed to the larger number of IBPs in $\mathbf{D_1}$, although $\pi-\pi$ interactions would be stronger than C−H/π ones at the same interatomic distance.

Atomic properties of the monomer are altered significantly in the crystal. For some properties, like $N(\Omega)$, the variations originated by geometry deformation are larger than those due to binding. The contrary is observed for properties related to electron density polarization. Variations of atomic properties upon binding in $\mathbf{D_1}$ indicate that (i) there is no global CT between monomers, (ii) there is a slight global polarization of $\rho(\mathbf{r})$ in each monomer, (iii) $\rho(\mathbf{r})$ tends to become slightly flatter upon stacking, (iv) atoms involved in stacking bond paths (or closely placed to them) experience the largest variations, and (v) $\rho(\mathbf{r})$ flattening mainly affects the distribution of the diffuse electron density placed far from the nuclei. In contrast, $\mathbf{D_2}$ formation takes place with a non-negligible CT (0.011 au) from $\mathbf{M^B}$ to $\mathbf{M^A}$, keeping in line with previous descriptions of IHB, where electron density is transferred from the base to the acid. Also, $\Delta^{b}N(\Omega)$ values are in line with those obtained for usual IHB complexes (particularly with C−H···O bonds). In $\mathbf{D_2}$, the main variations are restricted for $\mathbf{M^A}$ to atoms involved in IBPs, whereas they are much more extended throughout the whole $\mathbf{M^B}$ monomer.

Electron density deformation, $\Delta\rho(\mathbf{r})$, achieves very small extreme values in both dimers. In $\mathbf{D_1}$, most of the $\rho(\mathbf{r})$-enhanced regions are in the molecular plane, close to depletion ones, which are placed out of the molecular plane (at both sides). In $\mathbf{D_2}$, $\Delta\rho(\mathbf{r})$ displays two main characteristics: (i) the most significant depletion and enhancement regions are placed alternatively along the strongest IBP, with nearly cylindrical symmetry, typical of IHBs, and (ii) non-negligible $\Delta\rho(\mathbf{r})$ regions are localized in $\mathbf{M^A}$ around atoms involved in IBPs, whereas they are extended throughout the whole monomer in $\mathbf{M^B}$.

Finally, cooperative effects on binding energies are small in the tetramer, and they are hidden for bond properties and CT. Nevertheless, they are significant on atomic electron population (reaching 0.010 au for C4 in $\mathbf{M^A}$), with the largest contributions exhibited by atoms involved in $\pi-\pi$ or C−H/π bond paths.

Acknowledgment. We thank Centro de Supercomputación de Galicia (CESGA) for providing access to its computational facilities and Xunta de Galicia for funding this research through project INCITE08PXIB314224PR. N.O. thanks the University of Vigo for a predoctoral fellowship.

References and Notes

(1) Meyer, E. A.; Castellano, R. K.; Diederich, F. *Angew. Chem., Int. Ed. Engl.* **2003**, *42*, 1210.
(2) Müller-Dethlefs, K.; Hobza, P. *Chem. Rev.* **2000**, *100*, 143.
(3) Hunter, C. A.; Lawson, K. R.; Perkins, J.; Urch, C. J. *J. Chem. Soc., Perkin Trans. 2* **2001**, 651.
(4) Ḥobza, P. *Phys. Chem. Chem. Phys.* **2008**, *10*, 2581.
(5) Černý, J.; Hobza, P. *Phys. Chem. Chem. Phys.* **2007**, *9*, 5291.
(6) Šponer, J.; Riley, K. E.; Hobza, P. *Phys. Chem. Chem. Phys.* **2008**, *10*, 2695.
(7) Zhao, Y.; Truhlar, D. G. *Acc. Chem. Res.* **2008**, *41*, 157.

(8) Zhao, Y.; Truhlar, D. G. *J. Chem. Theory Comput.* **2007**, *3*, 289.
(9) González Moa, M. J.; Mandado, M.; Mosquera, R. A. *J. Phys. Chem. A* **2007**, *111*, 1998–2001.
(10) Matta, C. F.; Castillo, N.; Boyd, R. J. *J. Phys. Chem. B* **2006**, *110*, 563.
(11) Robertazzi, A.; Platts, J. A. *J. Phys. Chem. A* **2006**, *110*, 3992.
(12) Waller, M. P.; Robertazzi, A.; Platts, J. A.; Hibbs, D. E. *J. Comput. Chem.* **2006**, *27*, 491.
(13) Tsuzuki, S.; Fujii, A. *Phys. Chem. Chem. Phys.* **2008**, *10*, 2584.
(14) Caroll, M. T.; Bader, R. F. W. *Mol. Phys.* **1988**, *65*, 695.
(15) Koch, U.; Popelier, P. L. A. *J. Phys. Chem.* **1995**, *99*, 9747.
(16) Grabowski, S., Ed. *Hydrogen Bonding—New Insights*; Springer-Verlag: Dordrecht, The Netherlands, 2006.
(17) Stone, A. J. *Chem. Phys. Lett.* **1993**, *211*, 101.
(18) Tsuzuki, S.; Honda, K.; Uchimaru, T.; Mikami, M.; Fujii, A. *J. Phys. Chem. A* **2006**, *110*, 10163.
(19) Mandado, M.; Graña, A. M.; Mosquera, R. A. *Phys. Chem. Chem. Phys.* **2004**, *18*, 4391.
(20) Geometry here used for crystalline catechol was obtained from the Cambridge Crystallographic Data Center (Refcode: CATCOL13).
(21) Bader, R. F. W. *Atoms in Molecules, a Quantum Theory*; Oxford University Press: New York, 1990.
(22) Bader, R. F. W. *Chem. Rev.* **1991**, *91*, 893.
(23) Zhao, Y.; Truhlar, D. G. *J. Phys. Chem. A* **2005**, *109*, 4209.
(24) Frisch, M. J.; Trucks, G. W.; Schlegel, H. B.; Scuseria, G. E.; Robb, M. A.; Cheeseman, J. R.; Montgomery, J. A., Jr.; Vreven, T.; Kudin, K. N.; Burant, J. C.; Millam, J. M.; Iyengar, S. S.; Tomasi, J. J.; Barone, V.; Mennucci, B.; Cossi, M.; Scalmani, G.; Rega, N.; Petersson, G. A.; Nakatsuji, H.; Hada, M.; Ehara, M.; Toyota, K.; Fukuda, R.; Hasegawa, J.; Ishida, M.; Nakajima, T.; Honda, Y.; Kitao, O.; Nakai, H.; Klene, M.; Li, X.; Knox, J. E.; Hratchian, H. P.; Cross, J. B.; Adamo, C.; Jaramillo, J.; Gomperts, R.; Stratmann, R. E.; Yazyev, O.; Austin, A. J.; Cammi, R.; Pomelli, C.; Ochterski, J. W.; Ayala, P. Y.; Morokuma, K.; Voth, A.; Salvador, P.; Dannenberg, J. J.; Zakrzewski, V. G.; Dapprich, S.; Daniels, A. D.; Strain, M. C.; Farkas, O.; Malick, D. K.; Rabuck, A. D.; Raghavachari, K.; Foresman, J. B.; Ortiz, J. V.; Cui, Q.; Baboul, A. G.; Clifford, S.; Cioslowski, J.; Stefanov, B. B.; Liu, G.; Liashenko, A.; Piskorz, P.; Komaromi, I.; Martin, R. L.; Fox, D. J.; Keith, T.; Al-Laham, M. A.; Peng, C. Y.; Nanayakkara, A.; Challacombe, M.; Gill, P. M. W.; Johnson, B.; Chen, W.; Wong, M. W.; Gonzalez, C.; Pople, J. A. Gaussian 03, revision C.04; Gaussian, Inc.: Wallingford, CT, 2004.
(25) Williams, D. E.; Xiao, Y. *Acta Crystallogr., Sect. A* **1998**, *49*, 1.
(26) Zhao, Y.; Truhlar, D. G. *J. Chem. Theory Comput.* **2005**, *1*, 415.
(27) Bader, R. F. W. *AIMPAC: A suite of programs for the theory of atoms in molecules*; Mc Master University: Hamilton, Ontario, Canada, 1994.
(28) Biegler-König, F. W.; Schönbohm, J.; Bayles, D. *J. Comput. Chem.* **2001**, *22*, 545.
(29) Sinnokrot, M. O.; Sherrill, C. D. *J. Phys. Chem. A* **2006**, *110*, 10656.
(30) Matta, C. F.; Castillo, N.; Boyd, R. J. *J. Phys. Chem. B* **2006**, *110*, 563.
(31) Bader, R. F. W.; Ting-Hua, T.; Tal, Y.; Biegler-König, F. W. *J. Am. Chem. Soc.* **1982**, *104*, 946.
(32) Koch, U.; Popelier, P. L. A. *J. Phys. Chem.* **1995**, *99*, 9747.
(33) Vila, A.; Mosquera, R. A.; Hermida-Ramón, J. M. *J. Mol. Struct. (THEOCHEM)* **2001**, *541*, 149.
(34) Carroll, M. T.; Bader, R. F. W. *Mol. Phys.* **1988**, *65*, 695.
(35) Vila, A.; Mosquera, R. A. *Chem. Phys.* **2003**, *291*, 73.
(36) Rozas, I.; Alkorta, I.; Elguero, J. *J. Phys. Chem. A* **1997**, *101*, 4236.
(37) Vila, A.; Mosquera, R. A. *Int. J. Quantum Chem.* **2006**, *106*, 928.

JP906045F